Zhu et al. *Microsystems & Nanoengineering* (2025)11:154
https://doi.org/10.1038/s41378-025-01016-z

Microsystems & Nanoengineering
www.nature.com/micronano

ARTICLE Open Access

Nanocomposite biosensor tracks honokiol-induced oxidative stress dynamics in 3D hydrogel-cultured lung cancer cells

Yuxuan Zhu[1,2], Zhichao Huang[1], Shichao Tian[1], Qi Wang[3], Fan Wu[1], Jingwen Liu[4], Ping Wang[1,5], Hao Wan[1,5]✉, Liujing Zhuang[1,2]✉ and Deming Jiang[1,5]✉

Abstract

In cancer cells, higher reactive oxygen species (ROS) than normal cells were observed due to hypermetabolism. The redox balance in cancer cells relies on accordingly upregulated antioxidant capacity. By manipulating oxidation and antioxidant systems, chemotherapeutic drugs can selectively kill cancer cells without hurting normal cells. As three-dimensional (3D) in vitro models, such as spheroids and organoids, have become widely used in cancer research, traditional detection methods (e.g., absorption tests or titration) are inadequate for detecting in 3D environments. Thus, it is crucial to find a new method to detect oxidative stress of 3D in vitro cancer models. Here, a nanocomposite electrochemical biosensor was exploited to evaluate oxidative stress of cancer cells cultured in the 3D environment. The oxidation-regulatory capacity of honokiol, a Magnolia genus-derived anti-cancer molecule, was evaluated. A screen-printed electrode (SPCE) was modified with reduced graphene oxide (RGO) and platinum nanoparticles (Pt NPs) to get Pt NPs/RGO/SPCE. Then the gelatin methacrylate/reduced graphene oxide (GelMA/RGO) hydrogel was applied to immobilized NCI-H1975 in a 3D bionic environment to get NCI-H1975/GelMA/RGO/Pt NPs/RGO/SPCE. After optimizing the experiment condition, the Pt NPs/RGO/SPCE showed a detection threshold of 0.65 μM and a linear field from 1 to 10 μM for H_2O_2 detection while the NCI-H1975/GelMA/RGO/Pt NPs/RGO/SPCE sensitively responded to H_2O_2-induced oxidative stress. By utilizing the NCI-H1975/GelMA/RGO/Pt NPs/RGO/SPCE we found honokiol (a natural polyphenol constituent) inhibits NCI-H1975 by inducing oxidative stress. This simple cell-based electrochemical biosensor can in situ evaluate oxidative stress of 3D cancer models conveniently. It can also be easily extended to the study of the mechanism of action of other drugs and holds broad application prospects in the fields of new drug development and drug repurposing.

Introduction

Over the past half a century, extensive research indicates that reactive oxygen species (ROS) play an important role in cancer. ROS are small molecules from the partial reduction of molecular oxygen during oxygen consumption and cellular metabolism, for example, hydroxyl (OH·) and superoxide ($O_2^{\cdot-}$), hydrogen peroxide (H_2O_2), and hypochlorous acid[1–3]. Increased ROS levels have been observed in various cancers and are thought to be oncogenic. ROS-induced damage to DNA, protein, and lipids are related to genetic instability and tumourigenesis[4,5]. The abnormal concentration of ROS also activates signaling pathways about cancer cell survival, tumor progression, drug resistance, and driven DNA damage and genetic instability[6]. A precisely regulated antioxidant defense system in cancer cells can detoxify elevated ROS levels while maintaining pro-tumorigenic signaling and resistance to apoptosis. However, if the balance of redox

Correspondence: Hao Wan (wh1816@zju.edu.cn) or
Liujing Zhuang (zhuangliujing@zju.edu.cn) or
Deming Jiang (gemnjiang@zju.edu.cn)
[1]Biosensor National Special Laboratory, Key Laboratory for Biomedical Engineering of Education Ministry, Department of Biomedical Engineering, Zhejiang University, Hangzhou 310027, China
[2]State Key Laboratory of Transducer Technology, Chinese Academy of Sciences, Shanghai 200050, China
Full list of author information is available at the end of the article

© The Author(s) 2025
Open Access This article is licensed under a Creative Commons Attribution-NonCommercial-NoDerivatives 4.0 International License, which permits any non-commercial use, sharing, distribution and reproduction in any medium or format, as long as you give appropriate credit to the original author(s) and the source, provide a link to the Creative Commons licence, and indicate if you modified the licensed material. You do not have permission under this licence to share adapted material derived from this article or parts of it. The images or other third party material in this article are included in the article's Creative Commons licence, unless indicated otherwise in a credit line to the material. If material is not included in the article's Creative Commons licence and your intended use is not permitted by statutory regulation or exceeds the permitted use, you will need to obtain permission directly from the copyright holder. To view a copy of this licence, visit http://creativecommons.org/licenses/by-nc-nd/4.0/.

status was disturbed, ROS may exert a cytotoxic effect which induces malignant cell death.

It has been explored to selectively kill cancer cells without hurting normal cells by manipulating ROS levels and antioxidant systems[7]. On the one hand, increasing ROS levels to toxic levels and exhausting the antioxidant system can cause programmed cell death. Many chemotherapy drugs, including anthracyclines, cisplatin, bleomycin, arsenic trioxide, are known to increase ROS production and cause cancer cell death[8]. Arsenic trioxide can impair the respiratory chain and increase superoxide production, leading to cell death[9]. On the other hand, suppressing ROS levels could suppress pro-tumorigenic signaling and inhibit cancer cell survival. For example, diphenyleneiodonium (DPI), a flavoprotein inhibitor, can suppress NOX4-generated ROS production and cause pancreatic cancer apoptosis[10]. By overexpressing antioxidant SOD3, ROS production is inhibited which inhibited metastasis of breast cancer[11]. As aberrant ROS level ahead of cell death, developing a new method to assess the intracellular ROS level after treatment is meaningful in drug development and mechanical research.

Except for cancer, the excessive amount of ROS accumulation is also associated with neurodegenerative disease and autoimmune disease[12,13]. As a result, the measurement of the intracellular ROS can contribute to greater comprehension of not only cancer therapy but also other important human diseases. Since hydrogen peroxide (H_2O_2) is the most common representative of ROS studies due to its long lifetime, a number of analytical approaches are designed for H_2O_2 detection, including fluorescence[14], chemiluminescence[15,16], and electrochemical methods[17]. Due to the conveniences, quick-responding, less restrictive inspection, and low-cost position, the electrochemical technique is mostly applied[18,19]. Compared to enzymatic sensors, non-enzymatic sensors are more stable, cost-effective, and with no need to immobilize enzymes on the electrode surface[20,21].

Graphene, a novel two-dimensional carbon nanomaterial, has been found with good electronic conductivity, high specific surface area, rapid electron-transfer rate, and good biocompatibility[22–24]. Graphene has been used widely as robust scaffolds to form hybrid materials. Many noble metals have been reported with good catalysts for redox reactions with H_2O_2, including platinum, palladium, rhodium, ruthenium, and other metals[25–28]. Decoration of metal nanoparticles on graphene leads to better catalytic efficiency due to faster electron transfer between electrode and detection molecules and larger electrochemically active surface areas[29,30]. In consequence, the incorporation of graphene and Pt nanoparticles provides advanced catalysis to H_2O_2, enabling fast and sensitive detection of ROS[17,31,32]. For example, Zhang et al. reported an RGO-Pt/GCE sensor to measure the H_2O_2 release from living cells with good sensitivity[17]. Cells in a three-dimensional environment (such as spheroids, organoids, and cells with three-dimensional scaffolds) have been shown through research to exhibit characteristics closer to in vivo cells in terms of gene expression, drug resistance, and metabolic activity[33–36]. However, there is currently a lack of a cost-effective, easy-to-use, and in situ real-time monitoring biomimetic sensor specifically for reactive oxygen species in cells with a three-dimensional environment.

To address the above challenges, we constructed a non-enzymatic electrochemical sensor with cells immobilized in a three-dimensional scaffold, aimed at measuring intracellular oxidative stress induced by honokiol during lung cancer therapy. Screen-printed carbon electrode (SPCE) was modified with reduced graphene oxide (RGO) and Pt nanoparticles (Pt NPs) through physisorption and electrolytic deposition, respectively. A 3D culture system was applied to maintain cells' in vivo activity and enhance the cell integrity and electrode surface for better electron transfer[37]. Results showed that honokiol, a novel anti-cancer drug from a natural source, can promote ROS production and up-regulate oxidative stress, leading to observed lung cancer cell death. Increased reduction current, augmented ROS-positive cell population, and more cell death was found in NCI-H1975 after treatment of honokiol. The novel nanocomposite biosensor developed in this study has been demonstrated as an effective and time-efficient platform for monitoring oxidative stress dynamics in 3D hydrogel-cultured lung cancer cells. Significantly, this sensing system exhibits remarkable detection potential for hydrogel-encapsulated cellular models including tumor spheroids and organoids, showing comparable sensitivity in oxidative stress quantification. This breakthrough suggests extensive potential applications in integrated analysis of pathophysiological responses across various 3D cellular architectures, particularly for comprehensive evaluation of redox homeostasis in advanced drug screening platforms and personalized therapeutic models.

Experimental Methods

Reagents and apparatus

Graphene oxide (GO) was bought from XF NANO, lnc. (China). Potassium hexachloroplatinate ($K_2PtCl_6{\cdot}6H_2O$) was bought from Aladdin, lnc. (China). All other chemicals were of reagent grade and were used as received without any further purification. A 0.02 M phosphate buffer solution (PBS, pH 7.4) was used as the supporting electrolyte. All the solutions were prepared with doubly distilled water.

GelMA/GO hydrogel preparation

The wet bath method was used for preparing gelatin methacrylate (GelMA)/GO hydrogels with some modification[38]. After ultrasonic treatment for 5 min, GO aqueous suspensions reached homogenous in PBS solution and 0.1 g of GO was mixed in 100 mL PBS. The GelMA powder was dissolved in PBS as a 10% (w/v) solution, and the lithium phenyl-2,4,6-trimethylbenzoyl phosphinate (LAP) photoinitiator was dissolved in PBS as 0.5% (w/v). Before experiment, the GelMA solution and LAP solution were mixed in equal volume as 5% (w/v) and 0.25% (w/v), respectively. Then GelMA/GO hydrogels were produced by mixing to homogenous. After exposure to 405 nm UV light for 10 s, the GelMA/GO hydrogel was crosslinked firmly.

Preparation of the nanocomposite biosensor

Screen-printed carbon electrodes (SPCEs) were purchased from Zensor Research & Development Co., Ltd. (Taiwan, China). The working electrode of SPCEs was printed using carbon ink with a diameter of 3 mm, suitable for small volumes of reagents and samples. The counter electrode was printed with carbon while the reference electrode was printed with silver ink.

After ultrasonic treatment for 2 hours, GO suspension of 5 mg/ml was dispersed in doubly distilled water (ddH_2O) by ultrasonication for 2 h. 10 µl of GO suspension was cast onto an SPCE and dried at room temperature. By carrying CV in the range from -1.5 to 0 V at a scan rate of 50 mV/s in 2 mM K_2PtCl_6 solution containing 20 mM HCl, the Pt NPs were deposited evenly on the electrode surface with the supporting electrolyte of PBS (0.02 M, pH 7.4). After the CV procedure, the reduced graphene oxide (RGO) was restored from the GO precursor, with its structure and conductivity significantly enhanced. The modified electrode was then washed carefully with ddH_2O and dried at room temperature. The electrolyte solutions were bubbled with N_2 gas for deoxygenation during electrochemical studies. We added H_2O_2 into PBS solution to reach a gradient concentration from 1 uM to 1000 uM. For evaluating the sensitivity of the modified electrodes, we measured the concentration of H_2O_2 by DPV with magnetically stirring.

For immobilizing the NCI-H1975 cells in the 3D environment to mimic the in vivo status, about 5×10^6 viable cells per mL were collected in a serum-free medium. Then 6 µL cell suspension was dropped onto the surface of the SPCE and subsequently covered with 5 µL GelMA/GO solution. After exposure to 405 nm UV light for 10 s, the GelMA/GO hydrogel was crosslinked firmly to achieve cell immobilization for electrochemical measurements. GO in NCI-H1975/GelMA/GO can be reduced using the CV method, constructing NCI-H1975/GelMA/RGO, thereby further improving the sensing performance of the electrochemical sensor.

Morphology observation and Elemental mapping analysis

Electrodes with bare SPCE, Pt NPs/SPCE, and Pt NPs/RGO/SPCE were studied by scanning electron microscopy (SEM) (Utral 55, Zeiss). Furthermore, the elemental composition of the electrode surface was imaged and analyzed by energy dispersive X-ray spectroscopy (EDS). Modified electrodes were preserved in a vacuum box before observation.

Cell culture and oxidative stress detection

The human non-small cell lung cancer line, NCI-H1975, was purchased from American Type Culture Collection (ATCC). NCI-H1975 were cultured in RPMI 1640 medium (Thermo Scientific, Logan, UT) containing 5% fetal bovine serum (FBS) (Invitrogen, Carlsbad, CA, USA), 100 U/mL penicillin, and 100 µg/mL streptomycin in a 5% CO_2 incubator at 37 °C. When reached the logarithmic phase of growth, cells were collected for experiments.

Electrochemical detection of H_2O_2 released by cancer cells

We measured the oxidative stress of cells by the method of Xing et al.[37] with slight modifications. Electrochemical experiments were performed using a CHI660e electrochemical workstation. For detection of H_2O_2 released, NCI-H1975 cells were incubated in 6-well culture plates (Corning Costar, Corning, New York, USA). 5 days later, the medium was replaced with an FBS-free medium. Following cell culturing, cells from six wells of the 6-well plate were collected and mixed at a ratio of 20:20:60 (µL) for GO dispersion solution, cell resuspension, and GelMA hydrogel, respectively. Subsequently, 8 µL of the resulting mixture was precisely dispensed onto the working electrode of each Pt NPs/RGO/SPCE, followed by UV crosslinking to construct the NCI-H1975/GelMA/RGO/Pt NPs/RGO/SPCE system. Seven treatments were performed as follows: blank group without any treatment, treated groups with honokiol treatment of 5 µM to 80 µM (5 µM, 10 µM, 20 µM, 40 µM, 80 µM), and 80 µM honokiol supplement with 10 µM H_2O_2 enzyme for 24 hours. CV, DPV, EIS signals were recorded in 0.02 M PBS solution (pH 7.4). The DPV was recorded in a potential range between -0.35 V and 0.05 V with a pulse amplitude of 0.05 V, a pulse width of 0.05 s, and a pulse period of 0.2 s. The CV was scanned within a potential range from -0.4 V to +0.4 V with a scan rate of 100 mV/s.

Determination of intracellular ROS by cytometry

Intracellular ROS levels were monitored using 2′,7′-dichlorofluorescein diacetate (DCFH-DA). Human lung cancer (NCI-H1975) cells were seeded in a 6-well plate with a density of 2×10^5 cells/well. After incubation

overnight, cells were treated with honokiol for 24 h. Further, flow cytometry and fluorescence microscopy was applied for measuring the fluorescence intensity of the treated cells[39].

Detection of ROS by confocal microscopy

After honokiol treatment, human lung cancer (NCI-H1975) cells were encapsulated in GelMA/RGO construct. Then the construct was incubated with DCFH-DA probes for 1 hour in the dark. Before detection, the remaining DCFH-DA was removed with PBS three times. A confocal microscope (Olympus BX61, Japan) was used for imaging. The 3D reconstructed images were obtained by Z-stack.

Cell Viability assay

The cell counting kit-8 (CCK8, Dojindo, Japan) was used to monitor cell viability according to the product instruction. The NCI-H1975 cells (2000 cells/well) were seeded in 96-well plates with six replicate wells and treated with honokiol of different concentrations. For detection, 10 µl CCK-8 solution was added to each well. After incubation for 1 h, the absorbance was detected at 450 nm with a microplate reader.

Results and Discussions

Working principle of nanocomposite biosensor

Although a lot of modified biosensors have been fabricated for the detection of H_2O_2 with improved sensitivity, few studies have focused on applications to detect ROS generation in cells. The approach to assess the level of ROS through detecting H_2O_2 was previously produced was produced previously[39]. As shown in Fig. 1, we designed a nanocomposite biosensor for 3D hydrogel-cultured lung cancer cells in situ detection. Firstly the screen-printed carbon electrode was modified with RGO and platinum nanoparticles. Then cells were immobilized by RGO, GelMA, and PBS after exposure to UV light. Finally, we used the electrochemical workstation to detect H_2O_2 levels. After treated with drugs that increase ROS levels, a series of radical chain reactions would lead to cell apoptosis.

Chracterization of RGO and Pt NPs on electrode surface

Figure 2 shows the scanning electron microscopy (SEM) and energy dispersive X-ray spectroscopy (EDS) images depicting the morphology and elemental distribution of both bare and modified electrodes. As shown in Fig. 2a, laminar and granular structures of carbon were observed at the surface of the bare electrode. Meanwhile, in the EDS images, the lamellar and granular structures exhibited relatively high carbon (C) elemental distribution. After modification, randomly distributed bright spots were observed along with the GO sheets and on the SPCE surface[17]. From the image in Fig. 2c, a laminated structure of RGO is obtained. After electroreduction of Pt nanoparticles, there are a lot of Pt nanoparticles covered and well distributed on both the SPCE surfaces and RGO/SPCE surfaces (Fig. 2b, c). The EDS analysis revealed that the modified Pt NPs/SPCE and Pt NPs/RGO/SPCE electrodes exhibited significantly higher platinum (Pt) content compared to the bare SPCE electrode. The Pt nanoparticles were found with a size of 40 nm. The RGO-Pt blending nanocomposites are believed to enhance the relevant electrochemical detection.

Chracterization of the nanocomposite biosensor

CV, DPV, and EIS were used to measure the sensitivity of the modified Pt NPs/RGO/SPCE biosensors. Typical redox peaks with current peak values of 107.3 µA, 216.3 µA, and 265.5 µA, respectively, were found in the CV of bare SPCE, Pt NPs/SPCE, and Pt NPs/RGO/SPCE

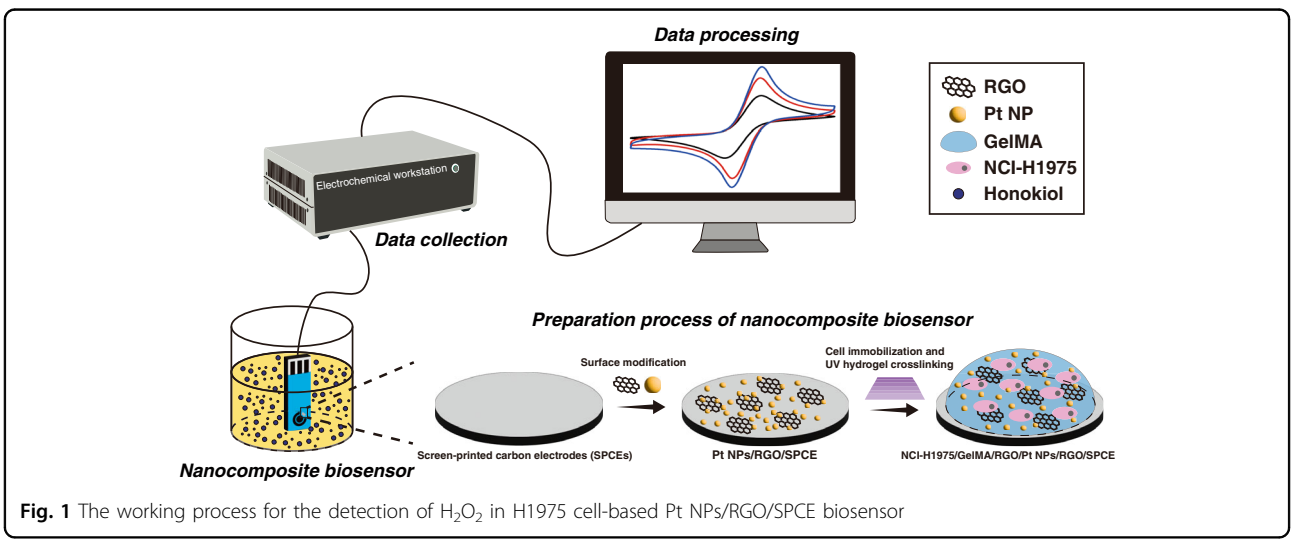

Fig. 1 The working process for the detection of H_2O_2 in H1975 cell-based Pt NPs/RGO/SPCE biosensor

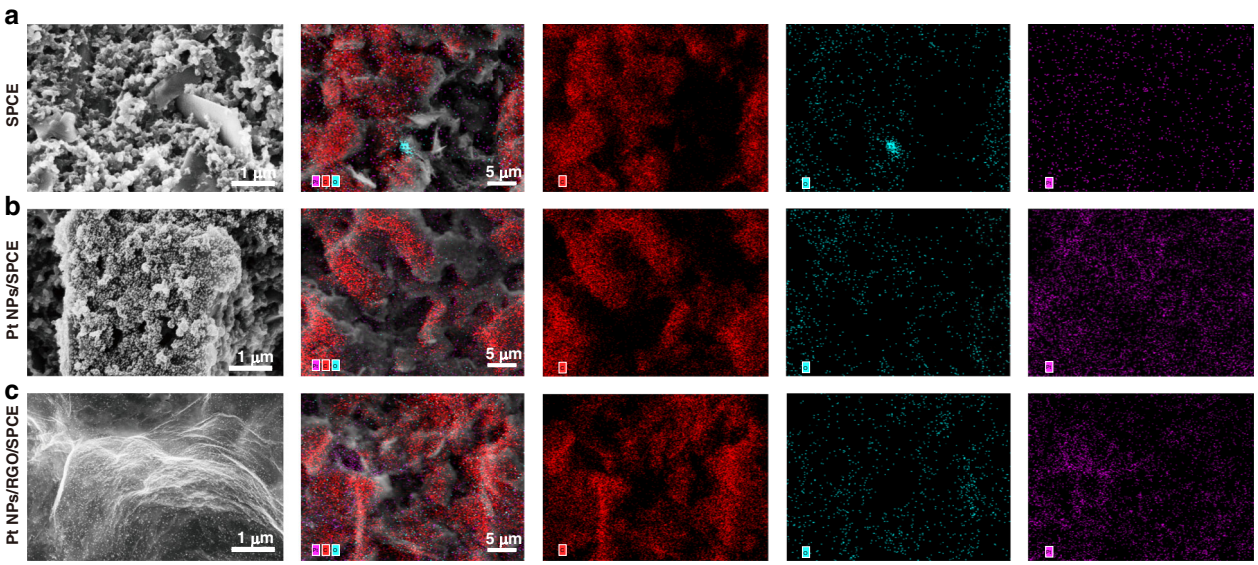

Fig. 2 SEM and EDS images of the surface of SPCE. a Pt NPs/SPCE **b** and **c** Pt NPs/RGO/SPCE

(Fig. 3b). Compared to RGO/SPCE and bare SPCE, Pt NPs/RGO/SPCE had a relatively higher current peak, better electric conducting property, and electro-sensitivity. After modified by hydrogels of GelMA/RGO and cells, the current decreased dramatically due to the increased charge transfer resistance in $Fe(CN)_6^{3-/4-}$ solution on the surface of the electrode. When the hydrogels and cells were fixed onto the electrode, conductivity decreased significantly.

The concentration of cells encapsulated inside the hydrogels was reported as the most important factor to impedance values[38]. The GelMA/RGO hydrogels containing a gradient of cells from $1 \times 10^3 \sim 1 \times 10^8$ cells/mL were used for the EIS experiment to select a suitable concentration (Fig. 3c, curve **d** to **h**). As shown in Fig. 3d, the increased cell concentration led to the increased stimulated R_{et} values. For the concentration from 10^3 to 10^6 cells/mL, a linear relationship between impedance was found with a correlation index of 0.992. However, the impedance tends to be stable when cell concentration above 10^6 cells/mL. No significant differences were found under 10^6, 10^7, and 10^8 cells/mL with the value of 1567 Ω, 1652 Ω, and 1764 Ω, respectively ($P > 0.05$). Thus, the concentration of 10^6 cells/mL was selected to evaluate the oxidant stress levels induced by honokiol.

An obvious reduction peak current appeared after the addition of H_2O_2 (1-7 mM), demonstrating that this peak was the signal of H_2O_2 (Fig. 4a). As increasing the concentration of the H_2O_2, the current peak value increased dramatically. For further exploring the detection characteristics, Fig. 4b shows the DPV curves of a gradient concentration of H_2O_2 (1-1000 μM). When $H_2O_2$was reduced, the peak appeared at around -0.14 V, which increased along with the increase of H_2O_2. As shown in Fig. 4c, the current increased quickly at low concentrations while slowly at high concentrations. A linear range from 1 to 10 μM was found in Fig. 4d. At every point of concentration, the RSD was found <5%. The linear equation was calculated as $Ip(\mu A) = 4.868\,C + 1.75$ with a correlation coefficient of 0.994. The limit of detection (LOD) was calculated to evaluate the performance. It was counted as $LOD = 3\,s/m$ where s represents the standard deviation of the blank sample and m represents the slope of standard lines. Here, the LOD was 0.65 μM with a sensitivity of 4.868 μA/μM. In conclusion, Pt NPs/RGO/SPCE is pretty sensitive for the investigation of H_2O_2 with a relatively simple fabrication process.

GelMA is an inexpensive and biocompatible hydrogel material derived from gelatin, a widely used biomaterial for tissue regeneration[40]. Cells easily bind to, elongate, proliferate, and migrate both when seed on GelMA scaffolds as well as when encapsulated in GelMA hydrogels. By modifying the methacrylate degree and gel concentration, the hydration and mechanical properties of GelMA can be altered for various applications. In the current study, 5% (w/v) GelMA and 0.25% (w/v) LAP were selected for encapsulating and maintaining cell activity. The SEM image of crosslinked GelMA showed a porous structure that appropriate cell survival (Figure S1). The porous and interconnected 3D structures of hydrogels are verified to aid the growth of the cells[41].

An important challenge for biosensors is the anti-interference ability. Glucose (Glu), oxalic acid (OA), and ascorbic acid (AA) were chosen as the interference in this study. In the solution containing 100 μM H_2O_2, the peak

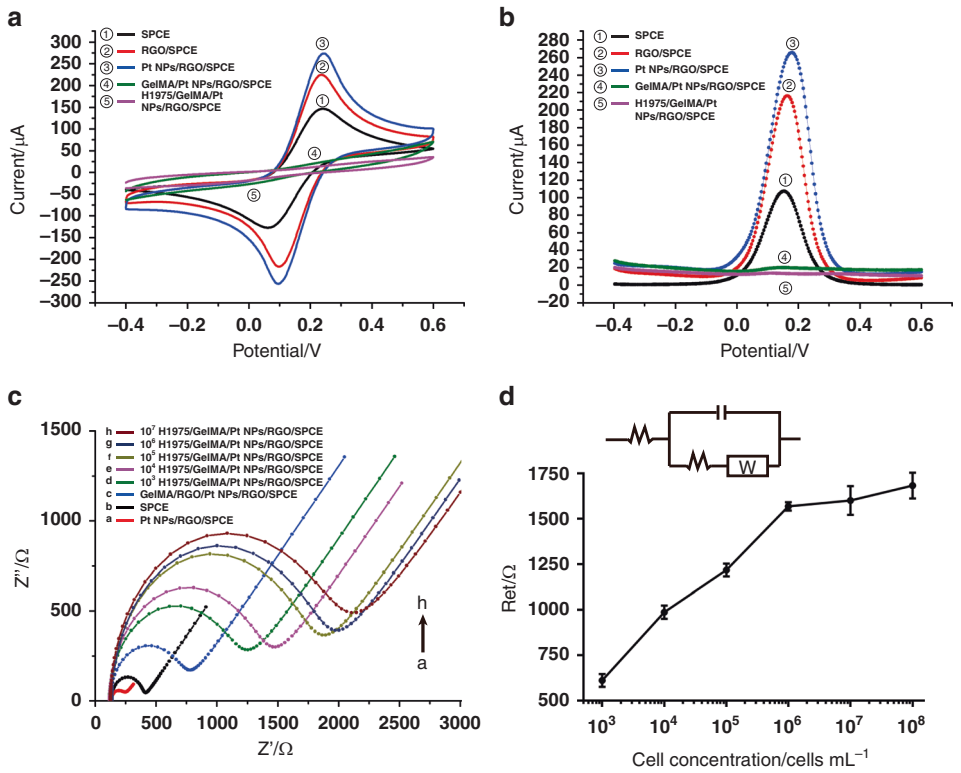

Fig. 3 Electrical characterization of nanocomposite biosensors. a Cyclic voltammograms and **b** differential pulse voltammetry results ① bare SPCE, ② RGO/SPCE, ③ Pt NPs/RGO/SPCE, ④ GelMA/Pt NPs/RGO/SPCE, ⑤ H1975/GelMA/Pt NPs/RGO/SPCE. **c** Nyquist diagrams of (a) Pt NPs/RGO/SPCE, (b) SPCE, (c) GelMA/RGO/Pt NPs/RGO/SPCE, (d) to (h): 1×10^3 to 1×10^7 cells/mL of NCI-H1975 cells immobilized on the electrodes. **d** R_{et} value when different concentration of cells were immobilized

value was 74.1 μA (Figure S2). After introducing the interference of Glu, OA, and AA, no significant differences in the peak values were found ($P > 0.05$). The results showed that the biosensor could keep good stability when used for H_2O_2 detection.

Honokiol regulates ROS level in H1975 cells

Honokiol is a phenylpropanoid molecule, which is detected in all parts of the Magnolia genus. Wide-range applications of honokiol are emerging, including neuroprotection, analgesia, anti-inflammation, and malignancy-control function[42]. Many factors participate in the regulation of tumor growth, progression, microenvironment, and metabolism. For example, the Notch signaling pathway is reported to have an important impact on glioblastomas multiforme cell growth[43]. Increased ROS level activates pro-tumorigenic signaling, while counter-intuitively ROS can also activate anti-tumourigenic signaling and initiate oxidative stress-induced tumor cell death[44]. Honokiol has been reported to control cancers by regulating ROS levels. In prostate cancer[45,46], honokiol can induce increased ROS production, while decreased ROS levels were detected in sarcoma[47] and breast cancer[48]. The mechanisms underlying these differences are not yet completely understood.

Aberrant level of ROS activates different cell death pathways, including apoptosis, autophagy, necrosis, and ferroptosis, to limit the cancer progression[49]. A study has verified that increased ROS production negatively regulates cellular FLICE-inhibitory protein (c-FLIP) post-transcriptionally, leading to death-inducing signaling complex (DISC) formation and subsequent activation of caspase cascade and apoptosis[50]. Besides, H_2O_2 has been shown to activate apoptosis signal-regulating kinase 1 (ASK1), inducing activation of the MAPK signaling pathway and the intrinsic pathway of apoptosis[51]. Metformin was reported to inhibit colorectal cancer by increasing ROS production, which suppressed the mTOR pathway and downstream targets S6 and 4EBP1[52]. Inhibition of ROS also involves tumor control. A mitochondrial sirtuin, SirT3, was found to control primary mouse embryo fibroblasts (MEFs) by suppressing ROS and regulating hypoxia-inducible factor 1α (HIF-1α)[53]. Iovine et al. demonstrated that treating colon cancer cells with carnosine would induce mitochondrial ROS, which was related to decreased ERK1/2 phosphorylation[54].

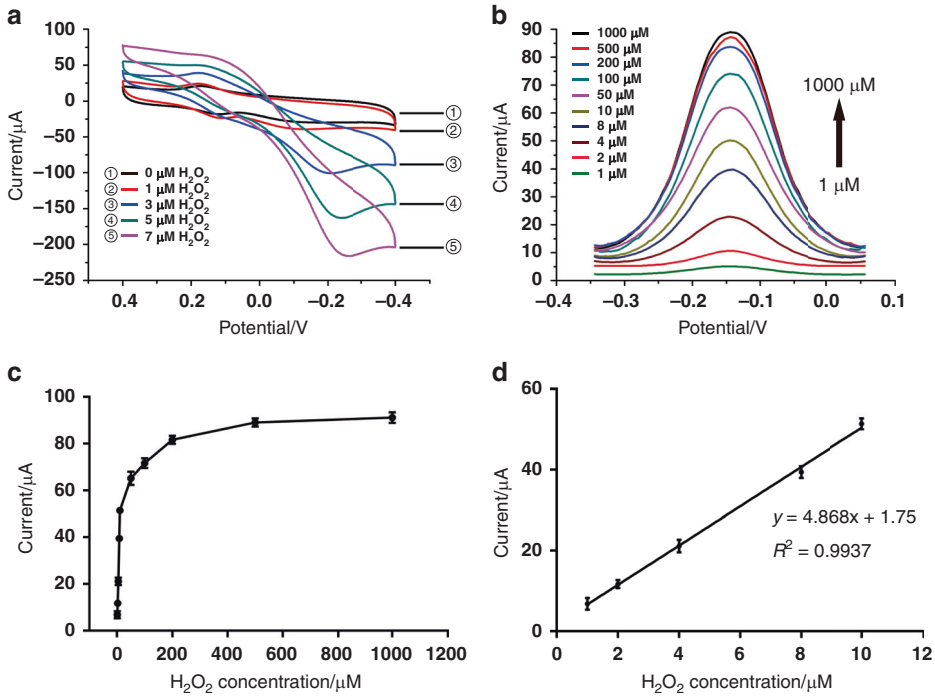

Fig. 4 Detection of H_2O_2 based on nanocomposite biosensors. a The CV responses of the Pt NPs/RGO/SPCE for detection of H_2O_2 (① 0 μM, ② 1 μM, ③ 3 μM, ④ 5 μM, ⑤ 7 μM). **b** The DPV responses of the Pt NPs/RGO/SPCE for detection of H_2O_2 (1 μM, 2 μM, 4 μM, 8 μM, 10 μM, 50 μM, 100 μM, 200 μM, 500 μM, 1000 μM). **c** The relation of the peak current and H_2O_2 concentration (1 μM, 2 μM, 4 μM, 8 μM, 10 μM, 50 μM, 100 μM, 200 μM, 500 μM, 1000 μM). **d** The linear relationship between the peak currents and H_2O_2concentrations (from 1 μM to 10 μM)

However, if ROS levels engaged in honokiol-induced lung cancer death is unclear. In this study, we evaluated honokiol-induced ROS levels in NCI-H1975 cells using our novel nanocomposite biosensor. Before encapsulating cells into RGO/GelMA hydrogels, six groups of NCI-H1975 cells were collected by trypsin and suspended in RPMI 1640 medium. Extensive studies have established GelMA as a prevalent 3D biomimetic scaffold that not only replicates the in vivo 3D microenvironment[55,56] but also maintains cellular gene expression patterns approximating native tissue states[57]. The encapsulation of H-1975 cells within RGO/GelMA hydrogels simulates their presence in a three-dimensional in vivo microenvironment. Given GelMA hydrogel's partial barrier effect on culture medium components, external substances gradually permeate into the hydrogel through diffusion. Unlike conventional two-dimensional cultures where drugs act at uniform concentrations, this permeation process creates a concentration gradient where effective drug molecules or nutrients maintain higher concentrations at the hydrogel periphery and lower concentrations in the central core region. When H-1975/RGO/GelMA constructs are exposed to honokiol-containing medium, peripheral H-1975 cells experience higher honokiol concentrations while centrally located cells encounter reduced drug levels. From a biomimetic perspective, this H-1975/RGO/GelMA system effectively replicates the drug permeation dynamics occurring in solid lung tumor tissues upon drug exposure, where pharmacological effects propagate throughout the tissue via gradual diffusion. The H_2O_2 detection system we developed based on H-1975/GelMA/RGO/Pt NP/RGO/SPCE can be optimized by simply replacing suspended H-1975 cells with H-1975 spheroids or patient-derived lung cancer organoids. Compared to the cell model constructed with suspended H-1975 cells in GelMA hydrogel that simulates the in vivo 3D microenvironment, using H-1975 spheroids increases the number of H-1975 cells within the GelMA hydrogel and better mimics drug penetration into the core region of spheroids, thereby more accurately reproducing the in vivo conditions of solid lung tumor tissues. Employing patient-derived lung cancer organoids as test models enables customized drug efficacy evaluation for individual patients. Consequently, our detection system demonstrates considerable application flexibility, serving as an efficient, cost-effective and convenient testing platform for early-stage drug evaluation, personalized medicine, and pharmacological mechanism research. We performed differential pulse voltammetry (DPV) to measure the current response of the H1975-based biosensor under varying concentrations of honokiol stimulation. As shown in Fig. 5a, b, the peak

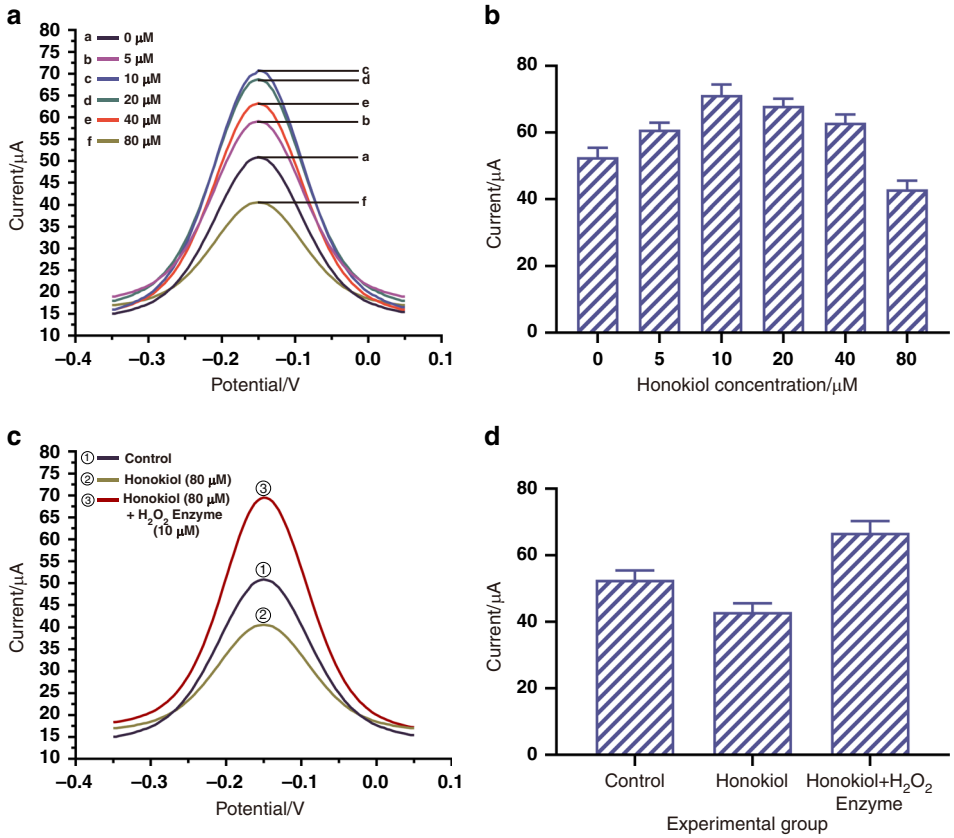

Fig. 5 Nanocomposite biosensors detect Honokiol-modulated ROS in H1975 cells. a The DPV responses of the H1975-based biosensor detected with different concentration of honokiol, a: 0 μM; b: 5 μM; c: 10 μM; d: 20 μM; e: 40 μM; f: 80 μM. **b** Peak values after treatment of honokiol ($n = 3$). **c** The DPV testing results of three distinct experimental groups: ①control (0 μM), ②Honokiol (80 μM), and ③Honokiol (80 μM) + H_2O_2 enzyme (10 μM). **d** The peak values of three distinct experimental groups

current of the 0 uM group was 50.85 μA. An interesting phenomenon was detected in the DPV results. The peak values for honokiol treatment ranged from 59.12 μA to 70.76 μA as the concentrations of 5 μM to 10 μM. However, as the concentrations increased further, the peak values decreased from 70.76 μA (10 μM) through 68.74 μA (20 μM) and 65.16 μA (40 μM) to 40.60 μA (80 μM). As shown in Fig. 5c, d, the addition of 10 μM H_2O_2 enzyme along with 80 μM honokiol increased the peak DPV response current from 42.62 μA (80 μM honokiol group) to 69.51 μA (80 μM honokiol + 10 μM H_2O_2 enzyme group). We speculate that this result may be attributed to the H_2O_2 enzyme decomposing portion of the honokiol-upregulated H_2O_2, thereby maintaining H1975 cells at a pro-growth oxidative level that increases cell numbers and consequently elevates total H_2O_2 production, leading to the observed current enhancement. In summary, the peak current results demonstrate an increase-decrease tendency with 10 μM as the threshold concentration of honokiol. Previous studies have reported that low concentrations of H_2O_2 benefit cells by activating multiple pathways including EGF, PDGF, and PTEN[58], while specifically enhancing tumor cell proliferation, metastasis and drug resistance[59]. As a plant-derived compound, honokiol exhibits diverse pharmacological effects—it activates the AMPK/SIRT1/PGC-1α pathway to protect peripheral nervous system[60] while concentrations ≥50 μM significantly increase oxidative stress to inhibit bladder cancer cell growth[61]. Although limited studies exist on honokiol's effects in lung cancer cells, most confirm its growth-inhibitory effects with varying IC_{50} concentrations (30–155 μM) across different cell lines and conditions[62], including enhanced viability in H358 cells at low concentrations. We therefore speculate that the observed biphasic peak current response may reflect honokiol's dual effects: promoting cell growth at low concentrations while suppressing viability through oxidative stress upregulation at higher concentrations in H-1975 cells.

For verifying the results of the cell-based biosensor, the ROS levels in NCI-H1975 cells were detected by flow cytometry and fluorimetry. As shown in Fig. 6b, 47.6% of

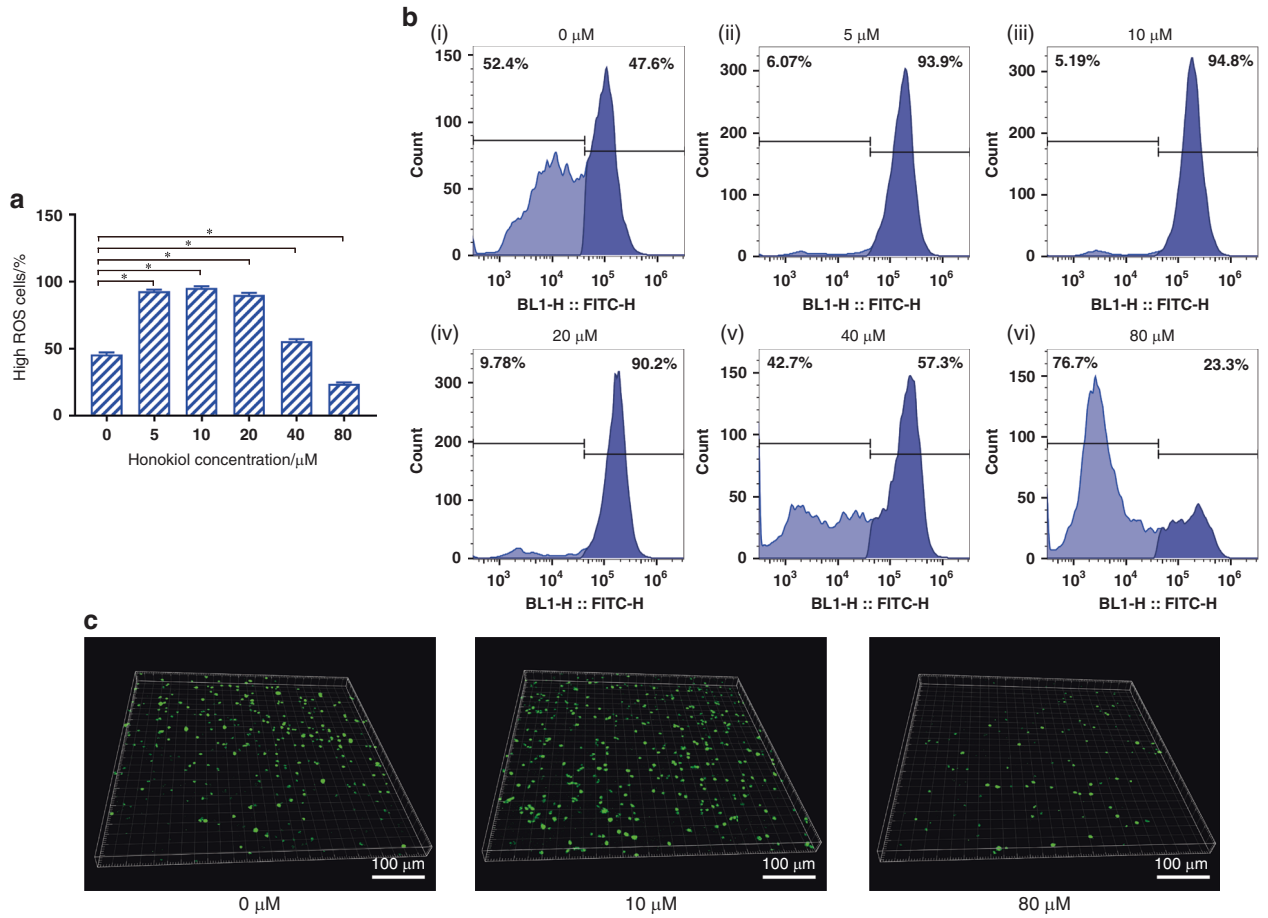

Fig. 6 Validation of Honokiol-mediated ROS modulation in H1975 cells. a Cell population of high ROS level after treatment with different concentration of honokiol by cytometry. (*$p < 0.05$, $n = 3$). **b** Results of cytometry after different treatment. **c** Fluorescence images of DCFH-labeled H1975 encapsulated in hydrogel and treated with different concentration of honokiol

cells without any treatment showed strong FITC signals, indicating this cell population had a relatively high ROS level. After treating cells with 5 μM and 10 μM honokiol for 24 h, the FITC-positive rate increased dramatically to as high as 93.9% and 94.8%, respectively. It demonstrated that honokiol treatment up-regulated oxidative stress significantly. A slight decrease of the FITC-positive population was observed when 20 μM honokiol was applied. As the concentration of honokiol increased further, a significant decrease in the FITC-positive population was detected. Only 57.3% and 23.3% of the population were counted for 40 μM and 80 μM of honokiol, respectively. Besides, cells encapsulated in hydrogels were imaged by a lazer confocus microscope. Relative high oxidative stress in cells led to the bright green fluorescence signals. As shown in Fig. 6c, cells exhibited different patterns after treating with honokiol of 0 μM, 10 μM, and 80 μM. Compared to the 0 μM group, more and enhanced green fluorescence signals were detected in the 10 μM group, while fewer and weaker signals were found in 80 μM group. The results of flow cytometry and fluorimetry indicated that with the increase in the concentration of honokiol, the intracellular ROS level went up first but then it went down, which is consistent with the electrochemical results. Meanwhile, our fabricated nanocomposite biosensor was verified to detect the intracellular ROS level accurately, quickly, and easily.

The puzzle was why the intracellular ROS levels decreased when the concentration of honokiol increased to 20 μM and higher. A reasonable assumption is that increased concentration of honokiol induced cell death, resulting in fluorescence decreased. In our study, a cell-permeable fluorescent and chemiluminescent probe, 2'-7'-dichlorodihydrofluorescein diacetate (DCFH-DA), was used for intracellular ROS detection. DCFH-DA is one of the most common tools for directly measuring intracellular redox state[63]. DCFH-DA is a non-fluorescent precursor of 2′-7′-dichlorofluorescein (DCF). After penetrating cells, DCFH-DA was cleaved by intracellular esterases and

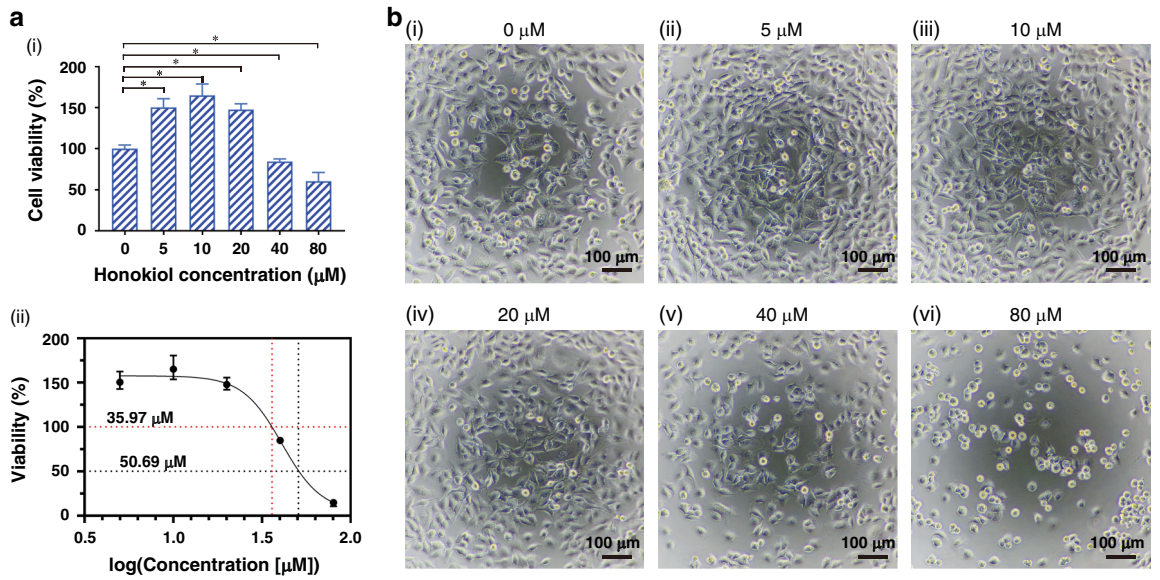

Fig. 7 Validation of Honokiol-mediated ROS impact on H1975 cell viability. a Cell viability test 24 h after treatment of honokiol, (i) CCK8 cell viability test bar graph, (ii) Fitting curve of honokiol's effect on H-1975. (*$p < 0.05$, $n = 3$). **b** The concentration images of cells after treatment of honokiol for 24 h (Scale bar = 100 μm)

subsequently oxidized to the fluorescent product DCF. The fluorescence signal relies on the intracellular enzyme system. High concentration induced cell death, which inhibits DCF formation and fluorescence signal. When the concentration of honokiol increased to 20 μM and a high level, significant cell inhibition probably occurred. Cell death led to the inactivation of the intracellular enzyme system, inhibiting the transformation of DCFH-DA to DCF.

For testing our hypothesis, cell viability was detected after treatment of honokiol for 24 h. As shown in Fig. 7a(i), honokiol of relatively low concentration (5, 10, and 20 μM) promoted cell proliferation significantly. Conversely, relatively high concentrations (40 and 80 μM) inhibit cells significantly. As shown in the fitting curve of the effect of honokiol on H-1975 in Fig. 7a(ii), at 35.97 μM, the effect of honokiol on H-1975 transitions from promoting cell growth to inhibiting cell growth. In addition, at 50.69 μM, honokiol exhibits a half-inhibitory effect on H-1975. Results could be observed intuitively under the microscope (Fig. 7b). Enhanced cell proliferation was observed in Fig. 7b(ii) to (iv), while lots of cell death were found in Fig. 7b(v) and (vi). This result confirms our hypothesis of that a high concentration of honokiol significantly inhibit cells and DCF formation. Here we supply a new method for the evaluation of anti-cancer drug-induced endocellular oxidative stress level. Based on the results, honokiol probably inhibits lung cancer cells through increasing intracellular ROS level.

Conclusion

Altogether, we have developed a nanocomposite biosensor to detect honokiol-induced ROS level through the fixation of live lung cancer cells on Pt NPs/RGO/SPCE. Due to the excellent catalytic characteristics of Pt NPs and RGO, a new type of biosensor for the effective detection of H_2O_2 with 0.65 μM LOD was constructed. In GelMA/RGO hydrogels, the NCI-H1975 cells showed a steady-state and have good cell viability when manufacturing biosensors. According to the peak current of DPV, the prooxidant potency of honokiol was evaluated. The results indicated that honokiol has a strong prooxidant capacity in lung cancer cells NCI-H1975. Honokiol increased intracellular ROS level with a concentration as low as 5 μM. Further increased ROS level significantly inhibited cell survival. Furthermore, combined with electrochemical tests, the production of ROS and cell viability were assessed. The intensity and population of flow fluorescence showed that honokiol treatment could promote the production of intracellular ROS. Increased ROS level induced observed cell death, which was directly verified with CCK8 and microscope images.

This approach is designed to develop novel technologies to test prooxidant properties on the basis of evaluating H_2O_2 levels of cells in the three-dimensional microenvironment. The propositioned cell-based electrochemotherapy has a significant edge over traditional trials and can be applied to precisely testing oxidant-regulation capacity of other anti-cancer drugs. This prompt, easy, and hypersensitized way to measure H_2O_2 easily from

living cells could be used to investigate the oxidant-regulation abilities of many other anti-cancer drugs, as well as for new drug discovery with promising application prospects.

Acknowledgements
This work was supported by National Natural Science Foundation of China (62120106004), Key Project of Zhejiang Province (2023C03104, 2024C03146), the Fundamental Research Funds for the Central Universities (226-2024-00059).

Author details
[1]Biosensor National Special Laboratory, Key Laboratory for Biomedical Engineering of Education Ministry, Department of Biomedical Engineering, Zhejiang University, Hangzhou 310027, China. [2]State Key Laboratory of Transducer Technology, Chinese Academy of Sciences, Shanghai 200050, China. [3]Center of Clinical Big Data and Analytics of the Second Affiliated Hospital and School of Public Health, Zhejiang University School of Medicine, Hangzhou 310058, China. [4]Department of Gastroenterology, the Second Affiliated Hospital, School of Medicine, Zhejiang University, Hangzhou 310009, China. [5]Cancer Center, Binjiang Institute of Zhejiang University, Hangzhou 310027, China

Data availability
Data will be made available on request.

Conflict of interest
The authors declare no competing interests.

Supplementary information The online version contains supplementary material available at https://doi.org/10.1038/s41378-025-01016-z.

Received: 28 February 2025 Revised: 29 May 2025 Accepted: 24 June 2025
Published online: 14 August 2025

References

1. Winterbourn, C. C. & Hampton, M. B. Thiol chemistry and specificity in redox signaling. *Free Radic. Biol. Med.* **45**, 549–561 (2008).
2. Dickinson, B. C. & Chang, C. J. Chemistry and biology of reactive oxygen species in signaling or stress responses. *Nat. Chem. Biol.* **7**, 504–511 (2011).
3. Manea, A. NADPH oxidase-derived reactive oxygen species: involvement in vascular physiology and pathology. *Cell Tissue Res.* **342**, 325–339 (2010).
4. Stanicka, J., Russell, E. G., Woolley, J. F. & Cotter, T. G. NADPH oxidase-generated hydrogen peroxide induces DNA damage in mutant FLT3-expressing leukemia cells. *J. Biol. Chem.* **290**, 9348–9361 (2015).
5. Szatrowski, T. P. & Nathan, C. F. Production of large amounts of hydrogen peroxide by human tumor cells. *Cancer Res.* **51**, 794–798 (1991).
6. Prasad, S., Gupta, S. C. & Tyagi, A. K. Reactive oxygen species (ROS) and cancer: Role of antioxidative nutraceuticals. *Cancer Lett.* **387**, 95–105 (2017).
7. Trachootham, D., Alexandre, J. & Huang, P. Targeting cancer cells by ROS-mediated mechanisms: a radical therapeutic approach? *Nat. Rev. Drug Discov.* **8**, 579–591 (2009).
8. Pelicano, H., Carney, D. & Huang, P. ROS stress in cancer cells and therapeutic implications. *Drug Resistance updates : Rev. commentaries antimicrobial anticancer Chemother.* **7**, 97–110 (2004).
9. Xin, X. et al. Inhibition of FEN1 increases arsenic trioxide-induced ROS accumulation and cell death: novel therapeutic potential for triple negative breast cancer. *Front. Oncol.* **10**, 425 (2020).
10. Mochizuki, T. et al. Inhibition of NADPH oxidase 4 activates apoptosis via the AKT/apoptosis signal-regulating kinase 1 pathway in pancreatic cancer PANC-1 cells. *Oncogene* **25**, 3699–3707 (2006).
11. Teoh-Fitzgerald, M. L., Fitzgerald, M. P., Zhong, W., Askeland, R. W. & Domann, F. E. Epigenetic reprogramming governs EcSOD expression during human mammary epithelial cell differentiation, tumorigenesis and metastasis. *Oncogene* **33**, 358–368 (2014).
12. Teismann, P. & Schulz, J. B. Cellular pathology of Parkinson's disease: astrocytes, microglia and inflammation. *Cell tissue Res.* **318**, 149–161 (2004).
13. Zhang, D. et al. High glucose intake exacerbates autoimmunity through reactive-oxygen-species-mediated TGF-β cytokine activation. *Immunity* **51**, 671–81.e5 (2019).
14. Belousov, V. V. et al. Genetically encoded fluorescent indicator for intracellular hydrogen peroxide. *Nat. methods* **3**, 281–286 (2006).
15. Wang, K., Liu, Q., Wu, X. Y., Guan, Q. M. & Li, H. N. Graphene enhanced electrochemiluminescence of CdS nanocrystal for H2O2 sensing. *Talanta* **82**, 372–376 (2010).
16. Tahirović, A., Copra, A., Omanović-Miklicanin, E. & Kalcher, K. A chemiluminescence sensor for the determination of hydrogen peroxide. *Talanta* **72**, 1378–1385 (2007).
17. Zhang, Y. et al. Highly sensitive graphene-Pt nanocomposites amperometric biosensor and its application in living cell H2O2 detection. *Anal. Chem.* **86**, 9459–9465 (2014).
18. Fan, W. T. et al. Stretchable electrode based on Au@Pt nanotube networks for real-time monitoring of ROS signaling in endothelial mechanotransduction. *Anal. Chem* **92**, 15639–15646 (2020).
19. Lyu, Q. et al. Real-time and in-situ monitoring of H(2)O(2) release from living cells by a stretchable electrochemical biosensor based on vertically aligned gold nanowires. *Anal. Chem.* **91**, 13521-13527 (2019).
20. Dhara, K. & Mahapatra, D. R. Electrochemical nonenzymatic sensing of glucose using advanced nanomaterials. *Mikrochimica Acta* **185**, 49 (2017).
21. Feizabadi, M., Soleymanpour, A., Faridnouri, H. & Ajloo, D. Improving stability of biosensor based on covalent immobilization of horseradish peroxidase by γ-aminobutyric acid and application in detection of H(2)O(2). *Int. J. Biol. Macromolecules* **136**, 597–606 (2019).
22. Huang, X., Qi, X., Boey, F. & Zhang, H. Graphene-based composites. *Chem. Soc. Rev.* **41**, 666–686 (2012).
23. Thangamuthu, M., Hsieh, K. Y., Kumar, P. V. & Chen, G. Y. Graphene- and graphene oxide-based nanocomposite platforms for electrochemical biosensing applications. *Int. J. Mol. Sci.* **20**, 2975 (2019).
24. Peña-Bahamonde, J., Nguyen, H. N. & Fanourakis, S. K. Recent advances in graphene-based biosensor technology with applications in life sciences. *Rodrigues DF* **16**, 75 (2018).
25. Yang, H., Wang, Z., Zhou, Q., Xu, C. & Hou, J. Nanoporous platinum-copper flowers for non-enzymatic sensitive detection of hydrogen peroxide and glucose at near-neutral pH values. *Mikrochimica Acta* **186**, 631 (2019).
26. He, S. B. et al. Highly sensitive colorimetric sensor for detection of iodine ions using carboxylated chitosan-coated palladium nanozyme. *Anal. Bioanal. Chem.* **412**, 499–506 (2020).
27. Gatselou, V. A., Giokas, D. L., Vlessidis, A. G. & Prodromidis, M. I. Rhodium nanoparticle-modified screen-printed graphite electrodes for the determination of hydrogen peroxide in tea extracts in the presence of oxygen. *Talanta* **134**, 482–487 (2015).
28. Deng, W. et al. Ruthenium ion-complexed carbon nitride nanosheets with peroxidase-like activity as a ratiometric fluorescence probe for the detection of hydrogen peroxide and glucose. *ACS Appl. Mater. Interfaces.* **11**, 29072–29077 (2019).
29. Hashemi, S. A. et al. Coupled graphene oxide with hybrid metallic nanoparticles as potential electrochemical biosensors for precise detection of ascorbic acid within blood. *Analytica Chim. Acta* **1107**, 183–192 (2020).
30. Khosroshahi, Z., Karimzadeh, F., Kharaziha, M. & Allafchian, A. A non-enzymatic sensor based on three-dimensional graphene foam decorated with Cu-xCu(2)O nanoparticles for electrochemical detection of glucose and its application in human serum. *Mater. Sci. Eng. C. Mater. Biol. Appl.* **108**, 110216 (2020).
31. Sun, Y., He, K., Zhang, Z., Zhou, A. & Duan, H. Real-time electrochemical detection of hydrogen peroxide secretion in live cells by Pt nanoparticles decorated graphene-carbon nanotube hybrid paper electrode. *Biosens. Bioelectron.* **68**, 358–364 (2015).
32. Liu, J., Bo, X., Zhao, Z. & Guo, L. Highly exposed Pt nanoparticles supported on porous graphene for electrochemical detection of hydrogen peroxide in living cells. *Biosens. Bioelectron.* **74**, 71–77 (2015).
33. Hoarau-Vechot, J., Rafii, A., Touboul, C. & Pasquier, J. Halfway between 2D and animal models: are 3D cultures the ideal tool to study cancer-microenvironment interactions? *Int. J. Mol. Sci.* **19** (2018).
34. Jensen, C. & Teng, Y. Is it time to start transitioning from 2D to 3D cell culture? *Front Mol. Biosci.* **7**, 33 (2020).

35. Wang, Y. & Jeon, H. 3D cell cultures toward quantitative high-throughput drug screening. *Trends Pharm. Sci.* **43**, 569–581 (2022).
36. Wang, Z. et al. Application of organoids in carcinogenesis modeling and tumor vaccination. *Front. Oncol.* **12**, 855996 (2022).
37. Xing, L. et al. Caco-2 cell-based electrochemical biosensor for evaluating the antioxidant capacity of Asp-Leu-Glu-Glu isolated from dry-cured Xuanwei ham. *Biosens. Bioelectron.* **105**, 81–89 (2018).
38. Jiang, D. et al. Preliminary study on an innovative, simple mast cell-based electrochemical method for detecting foodborne pathogenic bacterial quorum signaling molecules (N-acyl-homoserine-lactones). *Biosens. Bioelectron.* **90**, 436–442 (2017).
39. Koul, M. et al. Cladosporol A triggers apoptosis sensitivity by ROS-mediated autophagic flux in human breast cancer cells. *BMC Cell Biol.* **18**, 26 (2017).
40. Nichol, J. W. et al. Cell-laden microengineered gelatin methacrylate hydrogels. *Biomaterials* **31**, 5536–5544 (2010).
41. Teng, W. et al. A tough, precision-porous hydrogel scaffold: ophthalmologic applications. *Biomaterials* **35**, 8916–8926 (2014).
42. Rauf, A. et al. Honokiol: an anticancer lignan. *Biomed. Pharmacother.* **107**, 555–562 (2018).
43. Mao, H., Lebrun, D. G., Yang, J., Zhu, V. F. & Li, M. Deregulated signaling pathways in glioblastoma multiforme: molecular mechanisms and therapeutic targets. *Cancer Investig.* **30**, 48–56 (2012).
44. Moloney, J. N. & Cotter, T. G. ROS signalling in the biology of cancer. *Semin. Cell Dev. Biol.* **80**, 50–64 (2018).
45. Hahm, E. R. & Singh, S. V. Honokiol causes G0-G1 phase cell cycle arrest in human prostate cancer cells in association with suppression of retinoblastoma protein level/phosphorylation and inhibition of E2F1 transcriptional activity. *Mol. Cancer Therapeutics* **6**, 2686–2695 (2007).
46. Hahm, E. R., Sakao, K. & Singh, S. V. Honokiol activates reactive oxygen species-mediated cytoprotective autophagy in human prostate cancer cells. *Prostate* **74**, 1209–1221 (2014).
47. Angelini, A., Di Ilio, C., Castellani, M. L., Conti, P. & Cuccurullo, F. Modulation of multidrug resistance p-glycoprotein activity by flavonoids and honokiol in human doxorubicin- resistant sarcoma cells (MES-SA/DX-5): implications for natural sedatives as chemosensitizing agents in cancer therapy. *J. Biol. Regulators Homeost. Agents* **24**, 197–205 (2010).
48. Singh, T. & Katiyar, S. K. Honokiol, a phytochemical from Magnolia spp., inhibits breast cancer cell migration by targeting nitric oxide and cyclooxygenase-2. *Int. J. Oncol.* **38**, 769–776 (2011).
49. Galadari, S., Rahman, A., Pallichankandy, S. & Thayyullathil, F. Reactive oxygen species and cancer paradox: To promote or to suppress? *Free Radic. Biol. Med.* **104**, 144–164 (2017).
50. Wang, L. et al. The Fas death signaling pathway connecting reactive oxygen species generation and FLICE inhibitory protein down-regulation. *J. Immunol. (Baltim., Md : 1950)* **180**, 3072–3080 (2008).
51. Hatai, T. et al. Execution of apoptosis signal-regulating kinase 1 (ASK1)-induced apoptosis by the mitochondria-dependent caspase activation. *J. Biol. Chem.* **275**, 26576–26581 (2000).
52. Mogavero, A. et al. Metformin transiently inhibits colorectal cancer cell proliferation as a result of either AMPK activation or increased ROS production. *Sci. Rep.* **7**, 15992 (2017).
53. Bell, E. L., Emerling, B. M., Ricoult, S. J. & Guarente, L. SirT3 suppresses hypoxia inducible factor 1α and tumor growth by inhibiting mitochondrial ROS production. *Oncogene* **30**, 2986–2996 (2011).
54. Iovine, B., Iannella, M. L., Nocella, F., Pricolo, M. R. & Bevilacqua, M. A. Carnosine inhibits KRAS-mediated HCT116 proliferation by affecting ATP and ROS production. *Cancer Lett.* **315**, 122–128 (2012).
55. Nguyen, L., McCaughey-Chapman, A. & Connor, B. GelMA hydrogel as a scaffold to enhance the survival and differentiation of human induced lateral ganglionic eminence precursor cells. *J. Neurosci. Meth.* **405** (2024).
56. Roegiers, I. et al. GelMA as scaffold material for epithelial cells to emulate the small intestinal microenvironment. *Sci. Rep.* **15**. (2025).
57. Shah, N. et al. Gelatin methacrylate hydrogels culture model for glioblastoma cells enriches for mesenchymal-like state and models interactions with immune cells. *Scientific Rep.* **11**. (2021).
58. Gill, J. G., Piskounova, E. & Morrison, S. J. Cancer, oxidative stress, and metastasis. *Cold Sh. Q B* **81**, 163–175 (2016).
59. Ju, S. H. Y. et al. Oxidative stress and cancer therapy: controlling cancer cells using reactive oxygen species. *Int. J. Mol. Sci.* **25**. (2024).
60. Hu, M. et al. Honokiol attenuates high glucose-induced peripheral neuropathy via inhibiting ferroptosis and activating AMPK/SIRT1/PGC-1alpha pathway in Schwann cells. *Phytother. Res.* **37**, 5787–5802 (2023).
61. Hsiao, C. H. et al. Honokiol induces apoptotic cell death by oxidative burst and mitochondrial hyperpolarization of bladder cancer cells. *Exp. Ther. Med.* **17**, 4213–4222 (2019).
62. Luo, L. X. et al. Honokiol Induces Apoptosis, G1 arrest, and autophagy in KRAS mutant lung cancer cells. *Front Pharmacol.* **8** (2017).
63. Eruslanov, E. & Kusmartsev, S. Identification of ROS using oxidized DCFDA and flow-cytometry. *Methods Mol. Biol. (Clifton, NJ)* **594**, 57–72 (2010).